Diyala Journal of Engineering Sciences

Journal homepage: https://djes.info/index.php/djes

ISSN: 1999-8716 (Print); 2616-6909 (Online)

# Design and Validation of Portable Low-Cost ESP32-C6 Based Data Acquisition for Real-Time Power Monitoring and Experimental Data Collection

Sylvester Tirones*, Yue Hu

Department of Electrical Engineering, Shanghai Jiao Tong University, 200240 Shanghai, China

**ARTICLE INFO**

**Article history:**
Received: 25/01/2026.
Revised: 01/05/2026,
Accepted: 14/05/2026,
Available online: 15/06/2026

**Keywords:**
Portable data acquisition
Real-time power monitor
ESP32-C6 microcontroller
INA219 current sensor
Python-based application

**ABSTRACT**

*This paper presents a portable, customized low-cost data acquisition system using the ESP32-C6 microcontroller and the INA219 sensor. The use of traditional multi-meters is time-consuming and subject to human error, especially for experiments with longer durations, which require continuous logging and repeated readings. Manual data recording increases the risk of transcription mistakes and limits sampling resolution. Since DC systems have gained significant attention in recent years across renewable energy and IoT applications, the need for more accurate, automated DC power acquisition is increasingly critical. We conduct a comparative analysis of the INA219 sensor under low and elevated voltage applications to evaluate the accuracy of the INA219 sensor with the calibrated reference DC power supply. Our experiment indicates perfect linear correlation between power and current in both modes ($r \approx 1.000$ for low-power, $r = 0.992$ for high-power) applications, respectively. A Python-based application was developed to assess the data logging ability of the COOLTERM software. This application will perform statistical analysis of the time-series power measurement datasets, including a visual representation in graphical form to clearly display the energy trend in the DC power system. This system provides a practical solution for real-time power measurement across a variety of DC systems, including IoT applications, solar renewable energy, laboratory experimentation, and related DC power systems.*

## 1. INTRODUCTION

Every day, electronic equipment requires the use of DC power, ranging from portable to domestic and industrial scenarios. Similarly, the latest trend in power generation and distribution focuses on the use of DC power, and this makes it one of the top studies in recent years [1-2]. Understanding how to monitor and control the DC parameters is becoming critical. Data collection serves as the fundamental backbone for system analysis, where empirical data provides a formal representation of system behavior and operational characteristics [3]. Accurate measurement data is essential for evaluating system performance and conducting meaningful parametric analysis [4]. In power systems in particular, precise data acquisition is critical for reliable performance assessment through measured electrical parameters.

Several studies of existing implementations of microcontroller-based with INA219 sensors have been developed for various monitoring applications, including early detection of energy consumption anomalies in household appliances [5], battery management systems in electric vehicles [6], and solar panel performance monitoring [7]. The INA219 sensor has demonstrated utility in renewable energy applications. For instance, researchers have employed an INA219 sensor to measure voltage and current output from solar panels for energy harvesting [7], while others have combined INA219 sensors with BH1750 illuminance sensors as a cost-effective solution for monitoring solar panel electrical behavior [8]. In micro-power systems, ESP32 microcontrollers paired with INA219 sensors have been used for data acquisition and wireless transmission [9-10].

* Corresponding author's E-mail: stirones@sjtu.edu.cn
DOI: 10.24237/djes.2026.19201

Comparative sensor studies provide important insights into measurement accuracy. An experiment in [11] indicates that while the MAX471 sensor achieves 97.5% accuracy in voltage measurements, the INA219 sensor demonstrates superior current measurement accuracy at 90.39%. Similarly, the PZEM-004T sensor shows slightly lower accuracy (96.83% for voltage, 88.56% for current) but offers better measurement stability. Furthermore, the INA219 sensor is more accurate than the ACS712 sensor in current measurement applications [12]. A collection of recent IoT-based approaches has explored energy monitoring using ESP32 and INA219 modules [13-16]. Some systems have even incorporated ESP8266 microcontrollers with INA219 sensors and lithium-ion battery storage to enable energy sharing in local microgrids [17]. Despite these developments, many existing solutions lack system portability and environmental adaptability. Software-based visualization and statistical methods for the evaluation of the data are not mentioned.

To address these limitations, we introduce a portable ESP32-C6/INA219 data acquisition system with serial logging in the COOLTERM application. We developed a Python-based software to analyze the statistical performance of the measurement, as well as visualize different plots indicating different parameters of the power consumption. A comprehensive experimental test on both low and elevated voltage devices was conducted to analyze the accuracy of the INA219 sensor. This portable power acquisition system can be deployed to fields, including IoT deployments, remote device monitoring, laboratory-based, and general DC power measurement.

## 2. METHODOLOGY

### *2.1 System Design and Components*

The main system architecture consists of a INA219 current power sensor and the ESP32-C6 microcontroller. This circuit is responsible for providing measurement between the supply DC bus and the load DC bus, as illustrated in Figure 1. As shown, the INA219 sensor is connected between the positive line of the supply bus and the load bus to transfer electrical energy to the connected loads. A reliable voltage reading requires common grounding between all the connected component. The ESP32-C6 microcontroller receives the measured parameters from the INA219 through the I2C interface, which is the serial data (SDA) and serial clock (SCL) lines. The ESP32-C6 collects these parameters, processes the reading, and transmits the results through a universal serial bus (USB) to a computer. The computer on the other hand, ensures data logging, storing and processing. In our setup, a COOLTERM software is used to capture and record the incoming parameters of the INA219 sensor measurements.

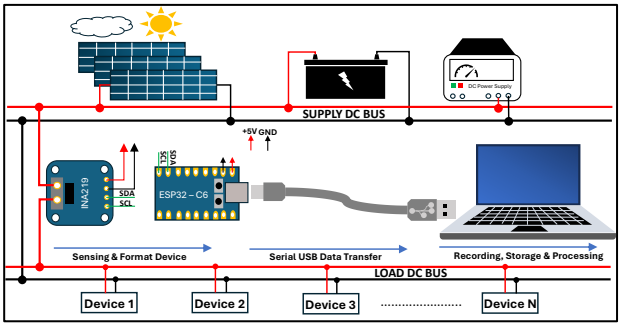


**Figure 1.** System architecture overview

A detail discussion on data logging procedure is presented in Section 2.4. It is noted that a computer has a large storage capacity, making it suitable for storing continuous time-series measurement data. The installation of MATLAB and Python software application can be deployed for data processing and visualization. A Python-based application and data processing capabilities are discussed in Section 2.7. This software ensures high quality data analysis and evaluation of the time-series electrical parameters of voltage, current, and power.

### *2.2 Hardware Configuration*

In this section, we discuss the main hardware setup of the ESP32-C6 and INA219 sensor. Firstly, the INA219 sensor is configured using its internal calibrated register. This ensures precision in the current and voltage measurement. The INA219 measures current by sensing the voltage drop across a precision shunt resistor. A 0.1 Ω shunt resistor was selected based on a comprehensive trade-off analysis considering measurement resolution, power dissipation, thermal stability, and the dual-range requirements as highlighted in Table 1 and 2. This selected resistor value provides optimal balance with 0.1 mA resolution. This is enough to cater for the 1.3 mA standby current. Consequently, it offers a voltage drop of 200 mV at max load (0.1Ω × 2A = 200 mV, or 1% of the 20V supply). Example of 0.01 Ω can be used for max current of 32A while 0.2 Ω will limit the max current and cause voltage drop and power dissipation as shown in Table 2. For our experiment, 16mW (3% of rating) and 400mW (80% of rating) at 2A continuous current is observed during low and elevated power mode, respectively. Thermal analysis indicates a maximum temperature rise of 40°C above ambient at full load, which remains within the resistor's 155°C operating limit and ensures measurement stability due to the ±50 ppm/°C temperature coefficient [18].

**Table 1.** Shunt resistor performance analysis

| Parameter | Low Power Mode (16V/400mA) | High-Power Mode (32V/2A) | Note |
|---|---|---|---|
| Maximum current | 400mA | 2A | Within INA219 limits |
| Full-scale shunt voltage | 40mV (0.1Ω×0.4A) | 200mV (0.1Ω×2A) | Within ±320mV ADC range |
| Resolution (12-bit ADC) | 0.1mA | 0.5mA | Sufficient for both applications |
| Power dissipation at max current | 16mV ($I^2R = 0.4^2\times 0.1$) | 400mV ($2^2\times 0.1$) | Acceptable for 0.5W rated resistor |
| Voltage drop at max current | 40mV | 200mV | <1% of supply voltage (acceptable) |
| Signal-to-noise ratio | 46dB | 60dB | Excellent for precision measurement |

**Table 2.** Shunt resistor trade-off analysis

| Shunt Value | Resolution (at 12-bit) | Max Current (320mA) | Power Loss at 2A | Suitability |
|---|---|---|---|---|
| 0.01Ω | 10 mA/LSB | 32A | 40mW | Too coarse for low-current measurement |
| 0.05Ω | 0.5mA/LSB | 6.4A | 200mW | Acceptable but lower resolution |
| 0.1Ω | 0.1mA/LSB | 3.2A | 400mW | **Optimal balance** |
| 0.2Ω | 0.05mA/LSB | 1.6A | 800mW | Exceeds 2A requirement, excessive power loss |
| 0.5Ω | 0.02mA/LSB | 0.64A | 2W | Current range insufficient for heater |

A detailed specification of INA219 is provided in Table 3. Similarly, the ESP32-C6 is a low-power microcontroller that supports Wi-Fi and Bluetooth, making it more reliable for portable applications. It supports peripherals such as GPIOs, UART/SPI/I²C, and ADC/DAC with built-in security features compared to other microcontrollers available in the market [19]. The ESP32-C6 operates as the inter-integrated circuit (I²C) master, supplying 3.3 V logic and controlling the SDA and SCL lines. The slaves are identified by their unique addresses, as shown in Figure 2. This setup also allows for multiple slave devices to connect to the master via I²C. The INA219 sensor has an address of 0x40. The I²C clock frequency is set to ensure steady communication and minimizing noise between the INA219 and ESP32-C6 during data transmission.

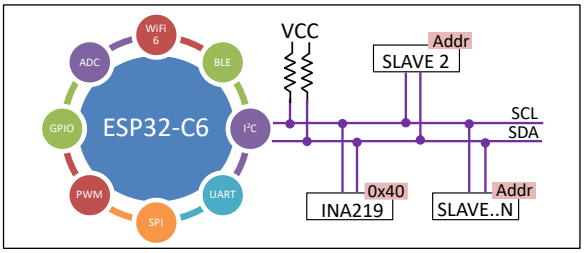


**Figure 2.** ESP32-C6 and INA219 I²C connection

The ESP32-C6 initializes the INA219 by applying a required calibration constant to measure electrical parameters at different load condition.

**Table 3.** INA219 current power sensor specification [20]

| Parameter | Specifications |
|---|---|
| Part number | INA219 (single-channel bi-directional current/power monitor) |
| Interface | I²C (two-wire) |
| Supply voltage | 3.0 V to 5.5 V (typical 3.3 V or 5 V systems) |
| Resolution | Current: ~0.1 µA (depends on shunt and configuration); Power: derived from current and voltage |
| Measurement range (shunt) | Programmable: ±40 mV (default) with internal gain to extend range; alternative configurations available via calibration |
| Bus voltage range | 0 V to 26 V (typical) |
| Power calculation | $P = V_{bus} \times I_{shunt}$ (internal calculation) |

The calibration setting of the INA219 is presented in Section 2.6. The ESP32-C6 processed these voltage and current reading internally before being transmitted to the host computer through the Universal Asynchronous Receiver/Transmitter (UART) serial interface. The UART is the protocol used for serial communication between the ESP32-C6 and a computer. Our hardware prototype of the portable ESP32-C6 data acquisition circuit is shown in Figure 3. The small dimension of the casing is 5×3.5×1.5cm, making it more flexible and portable. This overall setup enables real-time data transfer to the host computer, ensuring that all

measurements are captured without loss. The simplicity of our hardware configuration allows the system to be integrated into a variety of DC power measurement environments.

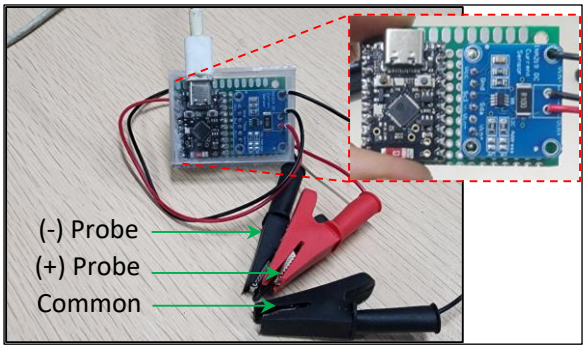


**Figure 3.** Prototype hardware development

*2.3 Firmware Workflow*

The ESP32-C6 firmware and pseudocode demonstrated in Figure 4 was developed to enable continuous data logging of electrical parameters measured by the INA219 sensor. The workflow begins with the initialization of the I²C interface, where the SDA and SCL pins are configured to enable communication between the ESP32-C6 and INA219 sensor. The INA219 calibration registers are then programmed to define the measurement range for bus voltage, shunt voltage, and current.

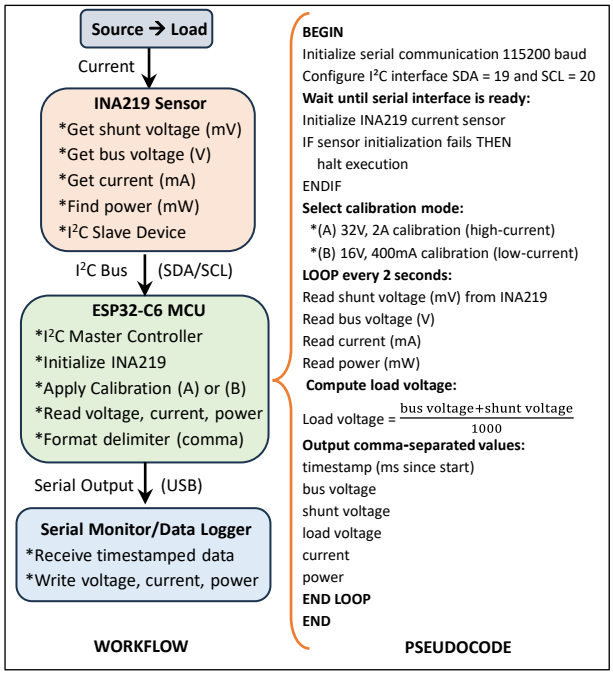


**Figure 4.** Data acquisition workflow

This programmable calibration mode is shown in the select calibration mode section of the pseudocode in Figure 4. Once the sensor is configured, the microcontroller enters a continuous reading mode. During each cycle, the ESP32-C6 reads the shunt voltage, bus voltage, and current values from the INA219. Instantaneous power is computed as the product of voltage and current values in the measurement. After processing, the ESP32-C6 formats the data into a comma-separated structure suitable for serial transmission. The UART serial link ensures that each measurement cycle is transmitted without loss, enabling accurate time-series logging. The USB connection between the microcontroller and the computer provides both power and a reliable communication channel for continuous measurement data transmission from the ESP32-C6 and the host computer. The firmware workflow is designed for prolonged measurement and logging. This approach supports real-time monitoring while maintaining the use of external logging software such as COOLTERM, which records the incoming time-series serial measurement of voltages, current, and power.

*2.4 Data Logging Procedure*

The data logging procedure occurs once the microcontroller transmits the processed INA219 measurements through the UART serial link. This incoming measurement data stream is captured using the COOLTERM software. This software is selected for its ability to record continuous serial data, apply time-stamping, and export logs in text or comma-separated formats (CSV) suitable for computation. The order of serial measurement transmitted data $S_i$ is given in (1). Similarly, serial receiver measurement data $M_i$ is shown in (2).

$$S_i = \sum_{i=1}^{n} P_{L,i}, I_{L,i}, V_{L,i}, V_{R,i}, V_{B,i}, t_i \quad (1)$$

$$M_i = \sum_{i=1}^{n} t_i, V_{B,i}, V_{R,i}, V_{L,i}, I_{L,i}, P_{L,i} \quad (2)$$

where,
$t$ = timestamp in ms,
$V_B$ = bus voltage,
$V_R$ = shunt voltage,
$V_L$ = load voltage,
$I_L$ = load current, and
$P_L$ = load power

The indexing $i$ of the format represents the specific data being transmitted and received. This approach is demonstrated in Figure 5.

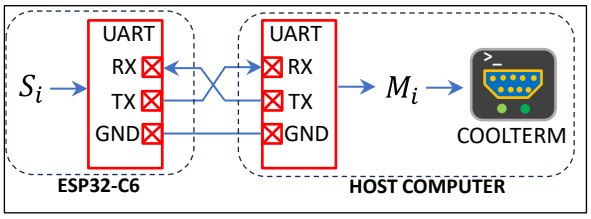


**Figure 5.** Serial data transmission format

The COOLTERM setup requires a baud rate and port selection to obtain the incoming $S_i$. During each transmission, it continues to record time-series

measurements of voltages, current, and power indexed into a dataset in the format of $M_i$. Each of these datasets can be stored locally and further imported into MATLAB or Python for visualization, statistical evaluation, and comparative analysis with the reference measurement.

*2.5 Experimental Setup*

The experimental setup was designed to evaluate the performance of the INA219-based data acquisition system under controlled laboratory conditions. A regulated DC power supply served as a reference instrument and a primary source for generating stable voltage levels, while two sets of resistive loads were used to draw measurable current. This structure of the logging procedure ensures reliable and consistent sensor reading for experimental validation. Figure 6 (a) and (b) illustrate the resistive loads setup of the DC low and elevated voltage experiment, respectively.

The low-power experiment was conducted to test and measure the power consumption of an atomizer circuit. This is to ensure that the INA219 sensor can accurately measure the low-power devices and record the data for processing. The atomizer circuit is powered by a 5V DC power source. The atomizer circuit operates in two distinct modes: 1) it operates using a push button switch, and 2) it operates using a PWM signal from a microcontroller. In this experiment, we used the push button to turn the atomizer on/off. The setup of this experiment is shown in Figure 6 (a). The atomizer is a device that converts water into vapor through high-frequency vibrations of piezoelectric plating [21]. The performance of the low-power device is similar and applicable to a micro-power system [9]. Similarly, a higher-power experiment was conducted to evaluate the sensor's performance under elevated current conditions. As demonstrated in Figure 6 (b), a PCB heater is employed. This PCB heater operates at a nominal voltage of 20V (within the extra-low voltage domain), making it a suitable candidate for evaluating the INA219 sensor under upper-range operating conditions for DC devices.

For the high-power measurement, the calibration is set to 32.0V and 2.0A. This setting enables fewer errors in the observation while increasing the accuracy of the reading through the INA219 sensor. On the other hand, the calibration of the low-voltage device is set to 16.0V and 400.0mA. In the entire experiment, voltage and current readings were collected at multiple operating points to enable comparative analysis and statistical evaluation.

*2.6 Calibration and Validation*

A DC Power Supply (Model No. GPD-3303S) was used as the reference instrument due to its widespread use in laboratory applications. We performed calibration to the INA219 sensor using the calibration setting in the ESP32-C6 firmware while applying a controlled voltage under different load conditions. These specific settings are present in Table 4. For each operating point, the INA219 measured bus voltage, shunt voltage, load voltage, and load current, while we simultaneously recorded the corresponding reference values.

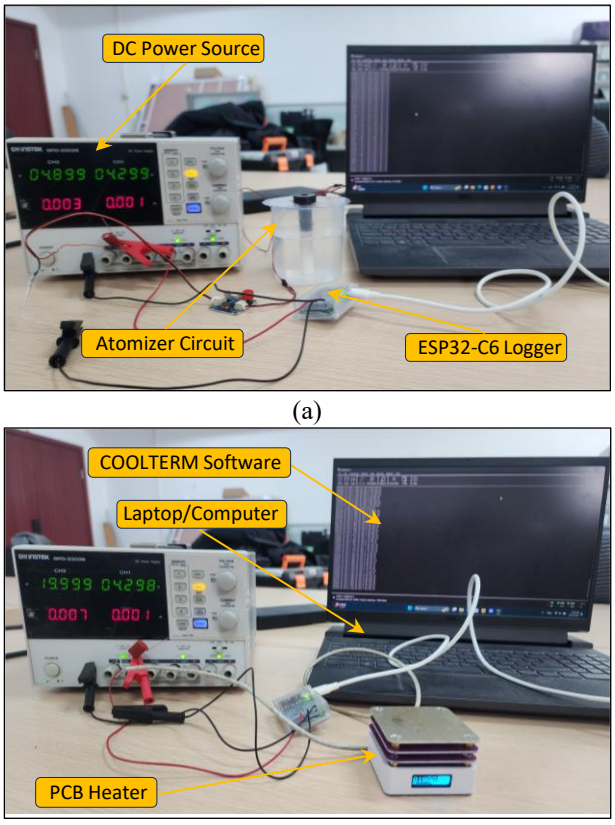


**Figure 6.** Laboratory experiment setup of (a) low current, and (b) elevated current operating mode

**Table 4.** Calibration of INA219 and reference setting

| Load Types | INA219 calibration | Calibrated DC Voltage |
|---|---|---|
| Low current | 16V/400mA | 5.0V |
| elevated current | 32V/2A | 20.0V |

This measurement approach is used to assess the accuracy of the INA219 sensor. To evaluate the performance of the INA219 sensor in the measurement, statistical metrics including mean absolute error (MAE), root-mean-square error (RMSE), and percentage deviation were calculated to justify the accuracy of the INA219 sensor. These mathematical statistics are further discussed in detail in Section 3.1. The validation procedure ensures the INA219 sensor can produce measurements comparable to those obtained from the DC power supply. It is recommended that the resulting error analysis support the assessment of the system's suitability for real-time power monitoring and experimental data collection applications.

*2.7 Software Data Processing*

We have developed a Python-based application that can analyze the time-series measurements of the datasets obtained from COOLTERM. Each dataset is then converted into numerical arrays representing voltage, current, and power values sampled during the experiment. Formatting of the raw serial log data can also be performed whenever necessary. MATLAB and Python are tools capable of effectively handling large datasets and facilitate reproducible analysis workflows.

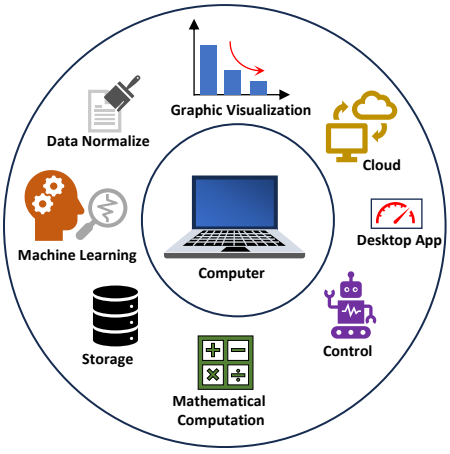


**Figure 7.** Data processing and visualization concept

Comprehensive treatments of data analysis in these environments can be found in [22] (MATLAB) and [23] (Python). The concept of our Python-based application into data analysis is illustrated in Figure 7, where measured data $M_i$ is computed into graphical and numerical representation, as well as storage and further processing. These comparisons and visualizations will greatly aid the measurement of behavior under different load conditions. In this study, we focus on the development of a Python-based application that has the ability to analyze the measurement in two modes: 1) Graphical representation, and 2) statistical analysis of the data.

The graphical representation of the data acquisition can plot the following identity:

(a) Power and current consumption over time using a line graph,
(b) Distribution of power consumption using histogram,
(c) Power consumption using a box plot,
(d) Voltage trend using a line graph,
(e) Power and current trend using colored Scatter graph

The graphical representation of our measurement is illustrated in Section 3.2. Similarly, this software can analyze the measurement dataset by applying statistical and numerical methods to evaluate the power consumption over time. The statistical formulation of the power measurement analysis is discussed in Section 3.1. Before analyzing how accurate a test is, it is vital to understand the types of data involved and how original studies describe and explain the test results, as these results can be shown using single numbers or combinations of measures [24].

*2.8 Statistical Distribution Analysis*

To understand the power consumption patterns in our experimental loads, we apply statistical distribution analysis methods. The dataset was first segmented into distinct operating modes based on current thresholds: off-state (I < 0.5 mA), standby mode (0.5 mA ≤ I < 10 mA), and active mode (I ≥ 10 mA for low-power; I ≥ 100 mA for high-power). Normality was analyzed using the Shapiro-Wilk test [25], which is appropriate for sample sizes n < 2000. A p-value < 0.05 indicates significant deviation from normality. Skewness ($\gamma_1$) and kurtosis ($\gamma_2$) were calculated using (3) and (4) respectively as:

$$\gamma_1 = \frac{\frac{1}{n}\sum_{i=1}^{n}(P_{L,i} - \bar{P}_L)^3}{\left(\frac{1}{n}\sum_{i=1}^{n}(P_{L,i} - \bar{P}_L)^2\right)^{3/2}} \quad (3)$$

$$\gamma_2 = \frac{\frac{1}{n}\sum_{i=1}^{n}(P_{L,i} - \bar{P}_L)^4}{\left(\frac{1}{n}\sum_{i=1}^{n}(P_{L,i} - \bar{P}_L)^2\right)^{2}} \quad (4)$$

These metrics quantify distribution shape, with skewness indicating asymmetry and kurtosis indicating tail weight. The power measurements and their corresponding values and indexing were interpreted following guidelines in [26].

## 3. RESULTS AND DISCUSSION

*3.1 Comparison between INA219 and Reference DC Power Supply*

The performance of the proposed INA219–ESP32-C6 data acquisition system was evaluated by comparing its measurements with those obtained from a calibrated DC power supply. Both low power and elevated power experiments were conducted to assess the sensor's accuracy across various operating ranges. Figures 8 and 9 illustrate the voltage and current comparison for low-power and elevated power conditions, respectively. To quantify the accuracy of the INA219 sensor, several statistical metrics were employed, including the mean ($\bar{x}$), mean absolute error (MAE), relative error (%), mean relative error, Pearson correlation coefficient ($r$), and coefficient of determination ($R^2$). These metrics help provides valuable comparative analysis into knowing the precision and linearity of our measurement. From (5), for the set of $n$ measurements of $x_i$ ($M_i$ and $R_i$), the mean is calculated as

$$\bar{x} = \frac{1}{n}\sum_{i=1}^{n} x_i \quad (5)$$

An example is that the mean of the INA219 current measurement data can be calculated using (6) as

$$M_i = \frac{I_1 + I_2 + \cdots + I_n}{n} \quad (6)$$

We aim to keep the difference between the INA219 measurement $M_i$ and the reference DC power supply value $R_i$ as small as possible. The MAE measures the absolute difference between reference $R_i$ and the actual $M_i$ INA219 sensor measurement, given in (7). If MAE$\leq|\bar{M}_i|$, then the model is performing well. That is, if MAE is less than or equal to the absolute magnitude of the mean of the INA219 sensor, the INA219 sensor is performing well [27]. This result is provided in Table 5 and 6 for low and elevated voltage measurements.

$$MAE = \frac{1}{n}\sum_{i=1}^{n} |M_i - R_i| \quad (7)$$

Relative and mean relative error (%) expressed as a percentage of the reference value is computed using (8) and (9), respectively. The relative error measures the accuracy of the measurement compared to the true value. The smaller the percentage of the relative error (%), the better the INA219 sensor is performing.

$$Rel.err\ (\%) = \frac{|M_i - R_i|}{R_i} \times 100 \quad (8)$$

It is noted that if $R_i = 0$ (e.g., zero current), the relative error is undefined. For the mean relative error (%) over $n$ samples, it is given as

$$Mean\ Rel.Err\ (\%) = \frac{1}{n}\sum_{i=1}^{n} \frac{|M_i - R_i|}{R_i} \times 100 \quad (9)$$

These statistical measures form the basis for evaluating the accuracy of the INA219 under different load conditions. They are implemented in the Python-based application to analyze the power measurement time-series datasets.

### *3.1.1 Low Voltage Reference Analysis*

The low-current application, such as the atomizer circuit, was categorized as a low-power device. The current and voltage measured were compared with the reference parameters of the calibrated DC power supply. From (10), it provides a mapping of the visual comparison of the INA219 sensor above and below the calibrated reference. The highlighted section of the graph is described as

$$color_{green,red} = \begin{cases} M_i > R_i, & green \\ M_i < R_i, & orange \end{cases} \quad (10)$$

where,
$M_i$ = INA219 parameter measurement,
$R_i$ = DC power supply measurement

Figure 8 demonstrates the visual data plotting of the experimental measurement. Figure 8 (a) and (b) show the voltage and current observation, respectively. The accuracy of the INA219 for low-power applications is analyzed using this observation. Table 5 and 7 summarizes the accuracy of the INA219 during low-power operation, segmented into three phases: standby, active operation, and zero-load conditions. In the low-power experiment, the INA219 demonstrated strong agreement with the reference supply for both voltage and current, given by the MAE and relative error in Table 5.

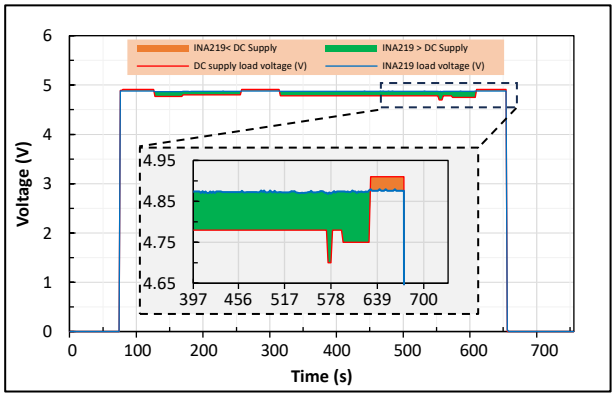


(a)

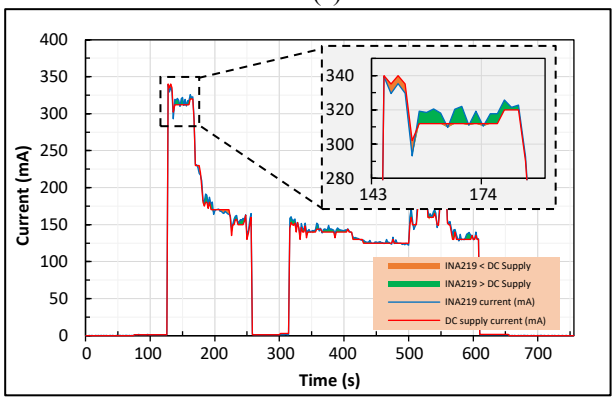


(b)

**Figure 8.** Comparative analysis of low-power experiment (a) voltage, and (b) current measurement

The highlighted regions in the comparison plots indicate instances where the INA219 measurement $M_i$ is greater than the reference value $R_i$ (red) or lower than the reference (green). These variations remained small and consistent, indicating stable sensor behavior under low-load conditions.

### *3.1.2 Elevated Voltage Reference Analysis*

Similar to the low current application, this experiment aims to determine the accuracy of the INA219 sensor under elevated current consumption (up to 2.8A). As highlighted in Figure 6 (b), a 20VDC PCB heater was used to observe how well the INA219 sensor can follow the calibrated DC power supply. Figure 9 (a) and (b) show the voltage and current measurement logging from the COOLTERM, respectively. For the high-power experiment, the INA219 also tracked the reference measurements closely as indicated in Table 6. A voltage drop to 11.45V was observed when the PCB heater was switched on, as shown in the zoom-in-

section Figure 9 (a). This is because the current of the DC voltage source was limited. During a current calibrated adjustment to 3A output, the voltage stabilized again at 20.0V. The INA219 captured this dynamic response accurately, demonstrating its suitability for monitoring rapidly changing loads.

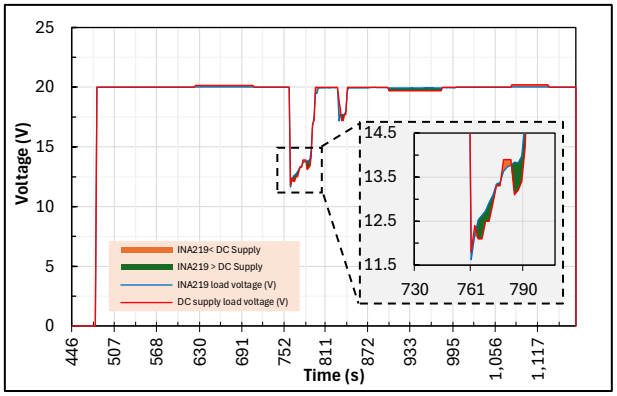


(a)

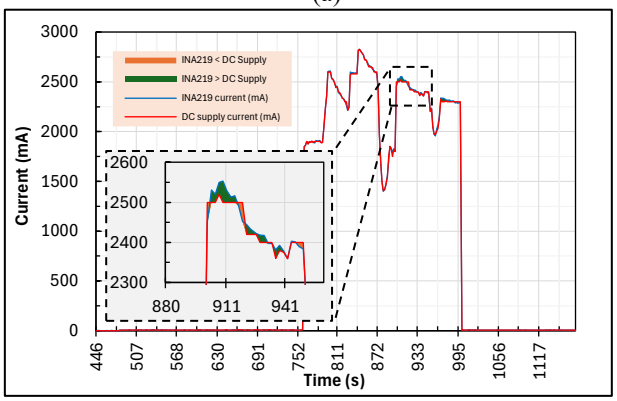


(b)

**Figure 9.** Comparative analysis of elevated-power experiment (a) voltage, and (b) current measurement

Overall, the comparison results confirm that the INA219 provides reliable measurements across both low and elevated power operating ranges, with deviations that remain within acceptable limits for portable power monitoring measurements and applications.

*3.1.3 Summary*

Provided in (11) is the statistical measure that quantifies the strength and direction of a linear relationship between the INA219 sensor and the DC power supply [28]. It is known as the Pearson correlation coefficient ($r$). We analyze this relationship in Table 7, highlighting the voltage and current correlation in the low and elevated voltage measurement.

$$r = \frac{\sum_{i=1}^{n}(M_i - \bar{M})(R_i - \bar{R})}{\sqrt{\sum_{i=1}^{n}(M_i - \bar{M})^2 \sum_{i=1}^{n}(R_i - \bar{R})^2}} \tag{11}$$

The range of $r$ indicates the relationship between the INA219 sensor and DC power supply, such that if:

$$r = \begin{cases} 1, & perfect\ positive\ correlation \\ 0, & no\ linear\ correlation \\ -1, & perfect\ negative\ correlation \end{cases} \tag{12}$$

On the other hand, the $R^2$ is used to evaluate the measurement in predicting the expected outcome. That means, a value of $R^2$ that is closer to 1 signifies greater accuracy of the measurement and is presented in (13) as

$$R^2 = 1 - \frac{\sum_{i=1}^{n}(R_i - M_i)^2}{\sum_{i=1}^{n}(R_i - \bar{R})^2} \tag{13}$$

**Table 5.** Accuracy and error analysis of low-power comparative measurement

| Status | Parameter | $\bar{M}_i$ | $\bar{R}_i$ | MAE | error (%) | Interpretation |
|---|---|---|---|---|---|---|
| Standby (min. power) | Voltage (V) | 4.877 | 4.90 | 00025 | 0.51 | Excellent voltage tracking |
| | Current (mA) | 1.29 | 1.28 | 0.03 | 2.3 | Very good low current accuracy |
| Active (max. power) | Voltage (V) | 4.87 | 4.78 | 0.092 | 1.93 | Good voltage accuracy |
| | Current (mA) | 165 | 160 | 8.5 | 5.3 | Moderate error, slight overestimate |
| Off-State (zero-state) | Voltage (V) | 0.002 | 0 | 0.002 | N/A | Accurate, minor noise |
| | Current (mA) | ±0.1 | 0 | 0.1 | N/A | Negligible zero-offset |

**Table 6.** Accuracy and error analysis of high-power comparative measurement

| Status | Parameter | $\bar{M}_i$ | $\bar{R}_i$ | MAE | error (%) | Interpretation |
|---|---|---|---|---|---|---|
| Standby (min. power) | Voltage (V) | 20.02 | 19.99 | 0.033 | 0.16 | Excellent voltage accuracy |
| | Current (mA) | 6.90 | 6.9 | 0.60 | 8.70 | Good agreement, slight noise |
| Active (max. power | Voltage (V) | 19.20 | 19.3 | 0.23 | 1.20 | Very good voltage tracking |
| | Current (mA) | 2450 | 2450 | 25.00 | 1.00 | Excellent elevated current accuracy |
| Off-State (zero-state) | Voltage (V) | 0.00 | 0.00 | 0.001 | N/A | Accurate |
| | Current (mA) | 0.70 | 0.00 | 0.70 | N/A | Minor zero-offset, negligible |

The accuracy of the INA219 sensor and reference for low and upper range voltage measurement is summarized in Table 7. This summary provides a key comparative analysis of the objective function of the INA219 sensor in low and elevated DC voltage applications. The INA219 performs exceptionally well at elevated power, with near-perfect linear correlation in both voltage and current measurements. Correlation uncertainties represent 95% confidence intervals (CI) calculated using Fisher's z-transformation.

Measurement uncertainties are combined standard uncertainties (k=1) derived from sensor specifications and experimental standard deviations. The near-perfect correlation (r ≈ 0.999) between current and power is expected due to the deterministic relationship P = V × I, with voltage remaining relatively stable during operation (coefficient of variation <1.5%). All correlation coefficients are statistically significant (p < 0.001).

**Table 7.** Summary of low and elevated power accuracy analysis

| Dataset | $r$ | $R^2$ | ± Uncertainty (95% CI) | Measurement uncertainty (±) | Interpretation |
|---|---|---|---|---|---|
| Low voltage correlation | 0.985 | 0.970 | ±0.008 | ±0.027V (0.56%) | Strong linear relationship |
| Low current correlation | 0.992 | 0.984 | ±0.005 | ±8.6mA (5.2%) | Excellent linearity |
| Elevated voltage correlation | 0.999 | 0.998 | ±0.001 | ±0.25V (1.3%) | Near-perfect linear tracking |
| high current correlation | 0.999 | 0.998 | ±0.001 | ±31.6mA (1.3%) | Excellent linearity |

*3.2 Data Processing and Visualization*

*3.2.1 Software Analysis and Visualization*

The analysis of the power consumption and its parameters can be performed using the data logging from the COOLTERM software. Python and MATLAB provide an environment that fully utilizes the statistical ability of the measured data. For this section, we employ Python-based software to recreate the data and assess the measurement by statistical and graphical representation. For the low-voltage atomizer circuit in Figure 6 (a), it was experimented with a 16V–400mA calibration mode, with its on/off operating intervals summarized in Figure 10 and Table 5.

The recorded power and current profiles capture the transitions between two operating states: (1) the atomizer switched on and produced mist, and (2) the atomizer switched off while the circuit remained energized. These transitions are reflected in the corresponding variations in measured power. The standard deviation in (14) measures the spread and variability of a measurement [29].

$$\sigma = \sqrt{\frac{1}{n}\sum_{i=1}^{n}(x_i - \bar{x})^2} \qquad (14)$$

It mostly assesses measurement noise and consistency within our dataset. Similarly, the high-power analysis is based on measurements from the PCB heater circuit, Figure 6 (b), using the 32 V–2 A calibration mode. The PCB heater on and off state, as shown in Figure 11 and Table 6, reveal two distinct operating conditions: 1) the heater switched on and actively heating the iron plating, and 2) the heater switched off while the supply remains connected.

That is, measurement is scaled by removing all the zero in the off-state with longer duration. This ensures we have a balance in the mean and median of the measurement in the high current operation state. As indicated in Table 8, high-power operation exhibits a significantly higher mean power consumption (31857.55mW) compared to low-power mode (483.80mW), with a correspondingly large standard deviation (20,242.77mW) indicating substantial load variability.

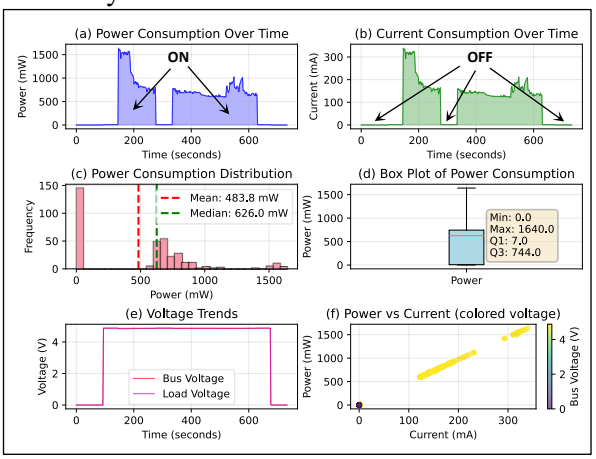


**Figure 10.** Python-based application for low power measurement and visualization.

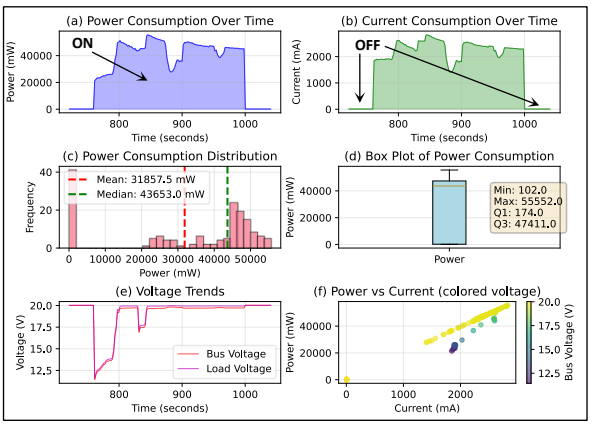


**Figure 11.** Python-based application for elevated power measurement and visualization

The dynamic change in the power consumption of the PCB heater shows a resulting fluctuation in the measurement and can be visually shown graphically. To avoid uncertainty in the distribution of the mean and median in the elevated current measurement, the data is normalized.

Low-power mode shows moderate variation (std. dev. = 446.91mW) with a median power (626.00mW) close to the mean, suggesting a relatively stable baseline load.

**Table 8.** Power consumption statistical analysis

| Parameters | Low power (mW) | Elevated power (mW) |
|---|---|---|
| Mean power | 483.80 | 31857.55 |
| Median power | 626.0 | 43653 |
| Min power | 0.0 | 102 |
| Max power | 1640.0 | 55552.0 |
| Standard deviation | 446.91 | 20242.77 |
| 25th percentile | 7.0 | 174.0 |
| 75th percentile | 744.0 | 47411.0 |

Current statistics in Table 9 reveal that high-power currents reach up to 2.83 A, with a mean of 1696.87 mA, while low-power currents remain below 340mA, with a mean of 99.71 mA. Negative current readings in low-power mode reflect sensor noise near zero load. The mean bus voltage is 3.95V and 18.99V while mean load voltage is 3.96 and 18.17 for low and elevated voltage measurement respectively. These voltage statistics indicate stable bus and load voltages in both modes, with high-power measurements averaging ~18.9 V and low-power measurements near 4 V.

Correlation Analysis shows an almost perfect linear correlation between power and current in both modes ($r \approx 1.000$ for low-power, $r = 0.992$ for high-power), confirming that current is the primary determinant of instantaneous power consumption in this system. Together, these tables provide distinct power characteristics and validate the INA219's ability to reliably monitor both low and elevated power applications with strong linear consistency.

**Table 9.** Current consumption analysis of low and elevated power measurement

| Parameters | Low current (mA) | Elevated Current (mA) |
|---|---|---|
| Mean current | 99.71 | 1696.87 |
| Min current | -0.20 | 6.10 |
| Max current | 339.40 | 2828.40 |

*3.2.2 Power Distribution Analysis*

The statistical distribution of power consumption reveals fundamentally different characteristics between low-power and high-power operation. As shown in Figure 10 and 11 and quantified in Tables 10 and 11, neither dataset follows a normal distribution when considered as a whole (Shapiro-Wilk $p < 0.001$), due to the multimodal nature of the measurements. The power distribution in Figure 10 (c) and 11 (c) is divided in operating modes as per low and elevated power measurement, as depicted in Table 11. For the low power distribution, we observed that the standby power has median = 7 mW, which exhibits significant right skew ($\gamma_1 = +2.34$) and high kurtosis ($\gamma_2 = 8.76$), indicating noise spikes above the baseline.

**Table 10.** Normality Test Results for Power Distribution

| Dataset | Mode | Shapiro-Wilk W | p-value | Normally Distributed? | Interpretation |
|---|---|---|---|---|---|
| Low Power | Standby | 0.892 | <0.001 | No | Multiple discrete state |
| | Active | 0.967 | 0.023 | No | Slight non-linearity |
| | Full Dataset | 0.621 | <0.001 | No | Bimodal distribution |
| Higher Power | Standby | 0.901 | <0.001 | No | Sensor noise floor |
| | Active | 0.983 | 0.087 | Yes | Near-normal during steady heating |
| | Full Dataset | 0.543 | <0.001 | No | Multimodal (off + active) |

**Table 11.** Skewness and Kurtosis Analysis

| Dataset | Mode | Skewness | Interpretation | Kurtosis | Interpretation |
|---|---|---|---|---|---|
| Low Power | Standby | +2.34 | Strong right skew (occasional noise spikes) | 8.76 | Leptokurtic (many outliers) |
| | Active | +0.42 | Mild right skew (more high-power events) | 2.89 | Mesokurtic (near-normal) |
| | Full Dataset | +3.12 | Strong right skew | 14.23 | Extreme leptokurtic |
| Higher Power | Standby | +1.89 | Moderate right skew | 6.54 | Leptokurtic |
| | Active | -0.23 | Mild left skew (slight voltage drop under load) | 2.67 | Mesokurtic |
| | Full Dataset | +1.45 | Moderate right skew | 4.32 | Leptokurtic |

Active mode power with mean = 803 mW shows near-mesokurtic behavior ($\gamma_2 = 2.89$) with mild right skew ($\gamma_1 = +0.42$), suggesting relatively stable consumption during atomizer operation with occasional higher-power events. Consequently, the active heating mode achieves near-normal distribution (Shapiro-Wilk $p = 0.087$, $\gamma_1 = -0.23$, $\gamma_2 = 2.67$), indicating stable, consistent power consumption during steady-state heating in the

elevated power distribution as observed in Table 11. The standby mode shows right skew ($\gamma_1 = +1.89$) due to occasional current spikes from the power supply. These distribution in our experiment validate the INA219's ability to capture both steady-state behavior and transient events, while highlighting the importance of segment mode for accurate power measurements. The following interpretation guide is used in Table 11.

- **Skewness = 0**: Perfectly symmetric
- **Skewness > +1**: Significant right skew (tail toward higher values)
- **Skewness < -1**: Significant left skew (tail toward lower values)
- **Kurtosis = 3**: Mesokurtic (normal distribution)
- **Kurtosis > 3**: Leptokurtic (heavy tails, many outliers)
- **Kurtosis < 3**: Platykurtic (light tails, few outliers)

*3.2.3 Power Consumption Summary*

The rolling average helps identify trends in our power consumption experiment. A moving average is a data smoothing technique used to identify trends in time-series or sequential data by reducing short-term fluctuations and highlighting longer-term patterns. For our power data sequences x[0], x[1], x[2]…x[k], the moving average at position $t$ is calculated using (15) [30].

$$MA_t = \frac{1}{k} \sum_{j=t-k+1}^{t} x_j \quad (15)$$

Where $k$ is the window size (number of samples), $\mathrm{MA}_t$ is the moving average at position $t$, and $x_j$ are the power measurement values.

The statistical significance of using the 5-samples provides a reasonable estimate of the central tendency and reduces the impact of our outlier power measurement, as shown in Figure 12 (a) and 13 (a) for low and elevated voltage measurement.

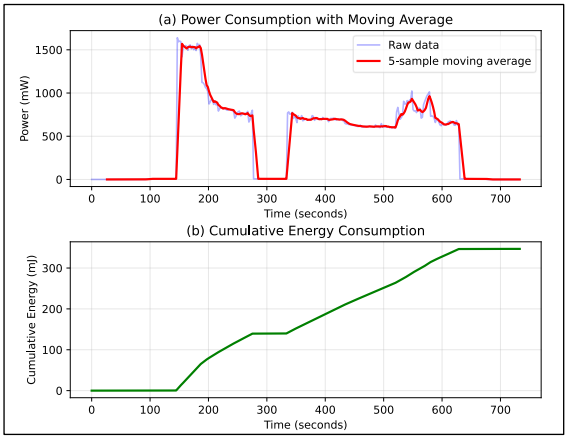


**Figure 12**. Python-based application for low-power energy trend.

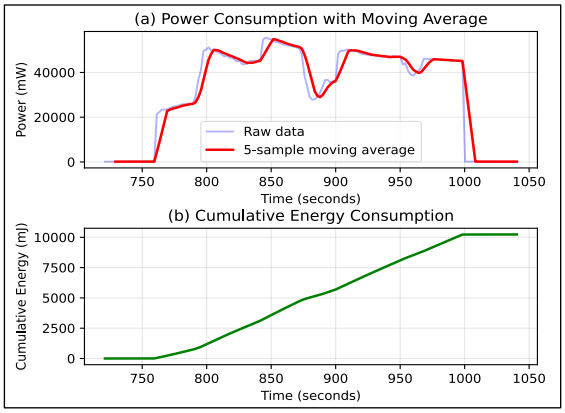


**Figure 13.** Python-based application for elevated power energy trend.

Table 12 shows the total energy consumed and the average power during the entire duration of our experiment.

**Table 12.** Overall energy and trend

| Measurement | Low power | Elevated power |
|---|---|---|
| Total energy used | 346.8mJ | 10234.9mJ |
| Average power | 0.47mW | 32.06mW |
| Measurement time | 133.02 sec | 319.27 sec |

*3.3 Comparative Analysis with Prior Work*

To contextualize the contributions and novelty of this work within the existing literature, Table 13 compares key specifications and capabilities of recent INA219-based data acquisition systems. Many of these studies in [5]-[17] focus on applications without comprehensive accuracy validation or statistical analysis. In our proposed work and experimental validation, we demonstrate several key advances as shown in comparison to other work in Table 13. These findings are highlighted as follows:

- we quantified voltage accuracy of 0.56-1.3%, exceeding previously reported values [11];
- we provide formal uncertainty analysis with 95% confidence intervals;
- we provide statistical distribution characterization including normality testing;
- dual-range validation across distinct operating modes; and
- we integrated Python-based analysis tools.

These findings position this work as a reference design for DC power monitoring application.

**Table 13.** Comparison of INA219-based data acquisition systems in recent literature

| Reference | Hardware Configuration | Voltage/Current Range | Sampling Rate | Accuracy/Error Metrics | Portability | Software Features | Key Applications |
|---|---|---|---|---|---|---|---|
| Korostenskyi & Olenych [5] | ESP32 + INA219 | Not specified | Not specified | Not quantified | Fixed installation | Local monitoring | Anomaly detection in appliances |
| Safril et al. [6] | ESP32 + INA219 | Battery voltage (3.7-4.2V) | Not specified | ±5% (estimated) | Vehicle-mounted | LCD display | EV battery management |
| Banerjee et al. [7] | STM32 + INA219 | 0-26V / 0-3.2A | 1 Hz | Not specified | Stationary | Serial monitor | Solar tracking |
| Romero-Sánchez et al. [8] | Arduino + INA219 + BH1750 | 0-20V / 0-3.2A | 0.5 Hz | Not quantified | Benchtop | Serial monitor | Solar panel monitoring |
| Wang et al. [9] | ESP32-S3 + INA219 | 3.3-5V / 0-1A | 10 Hz | Not specified | Benchtop | MQTT dashboard | Micro-power systems |
| Crowter & Saeed [10] | ESP32 + INA219 | 0-15V / 0-2A | 1 Hz | ±2% (claimed) | Portable enclosure | Web interface | PV battery monitoring |
| Sari et al. [11] | ESP32 + INA219 (comparative) | 0-20V / 0-5A | Not specified | Voltage: 97.5% accuracy; Current: 90.39% accuracy | Benchtop | Serial monitor | Sensor accuracy comparison |
| Maroșan et al. [12] | Raspberry Pi + INA219 + ACS712 | 0-26V / 0-3.2A | 10 Hz | INA219: ±0.5% (claimed) | Benchtop | Node-RED dashboard | Sensor comparison |
| Gaikar et al. [13] | Arduino + INA219 | 0-20V / 0-3.2A | 1 Hz | Not quantified | Fixed installation | ThingSpeak cloud | Solar energy monitoring |
| Hakim et al. [14] | ESP32 + INA219 | Battery voltage (3.7-12V) | 5 Hz | Not specified | Portable | Blynk app | Battery consumption monitoring |
| Luechaphonthara & A [15] | ESP8266 + INA219 | 0-26V / 0-3.2A | Not specified | Not quantified | Fixed installation | Web dashboard | Home appliance monitoring |
| Salunkhe et al. [16] | ESP32 + INA219 | 0-26V / 0-3.2A | 1 Hz | Not specified | Benchtop | Blynk app | Smart energy meter |
| Patel et al. [17] | ESP32 + INA219 | 0-24V / 0-3.2A | 2 Hz | Not specified | Benchtop | Local display | Peer-to-peer energy grid |
| This Work | ESP32-C6 + INA219 | 5V (0-340 mA) and 20V (0-2800 mA) | ~2 Hz | Voltage: 0.56-1.3% error; Current: 1.3-5.2% error; $R^2$ = 0.984-0.998 | Portable (5×3.5×1.5 cm) | COOLTERM, Python-based analysis with statistical tools | Dual-range DC power monitor with uncertainty analysis |

## 4. CONCLUSIONS

This paper presented a portable, low-cost data acquisition system combining an INA219 sensor with an ESP32-C6 microcontroller for real-time DC power monitoring. The system was experimentally validated across two distinct operating regimes: low-power (5V, 0-340 mA) and elevated-power (20V, 0-2800 mA) applications. Key quantitative findings include:

- **Measurement accuracy:** Mean absolute error of 0.09 V (0.56%) for low-voltage and 0.23 V (1.3%) for elevated-voltage measurements, with current errors of 8.5 mA (5.2%) and 25 mA (1.3%) respectively.
- **Linear correlation:** Near-perfect linearity between current and power in both regimes ($R^2$ = 0.984 for low-power, $R^2$ = 0.998 for elevated-power), confirming power as a deterministic function of current with stable voltage operation.
- **Uncertainty analysis:** Combined standard uncertainty of ±0.024 V (low-power) and ±0.101 V (elevated-power), with expanded uncertainties (k=2) of ±0.048 V and ±0.202 V respectively at 95% confidence.
- **Statistical distribution:** Active heating mode achieved near-normal distribution (Shapiro-Wilk p = 0.087, skewness = -0.23), while standby modes exhibited significant right skew due to occasional noise spikes.
- **Form-factor:** The complete system measures 5 × 3.5 × 1.5 cm, enabling deployment in space-constrained applications.

The developed Python-based application provides automated statistical analysis and visualization capabilities, transforming raw serial data into actionable insights through histogram analysis, distribution characterization, and energy trend visualization.

## REFERENCES


[1] S. Saha and S. Roy, "Design and implementation of a smart energy meter with demand response capability," in *Proceedings of the 2016 ACEEE Summer Study on Energy Efficiency in Buildings*, 2016, pp. 1–12. [Online]. Available: https://www.aceee.org/files/proceedings/2016/data/papers/1_156.pdf

[2] S. Tirones and Y. Hu, "Design and analysis of a wide-input-range (5V–12V) buck converter for stable 5V/1A USB charging: A Simulink approach," *Int. Res. J. Adv. Eng. Sci.*, vol. 10, no. 3, pp. 121–127, 2025.

[3] N. Nissa, S. Jamwal, J. I. Bhat, and Y. Rashid, "Data collection and analysis: The foundation of evidence-based research in various disciplines," in *Intelligent Signal Processing and RF Energy Harvesting for State of art 5G and B5G Networks*, J. A. Sheikh, T. Khan, and B. K. Kanaujia, Eds. Singapore: Springer, 2024, pp. 185–205. doi: 10.1007/978-981-99-8771-9_9.

[4] A. Razumić, B. Runje, V. Alar, B. Štrbac, and Z. Trzun, "A review of methods for assessing the quality of measurement systems and results," *Appl. Sci.*, vol. 15, no. 17, p. 9393, 2025. doi: 10.3390/app15179393.

[5] R. Korostenskyi and I. Olenych, "EDGE approach to early detection of anomalies in electricity consumption," in *2025 IEEE 6th KhPI Week on Advanced Technology (KhPIWeek)*, Kharkiv, Ukraine, 2025, pp. 1–5. doi: 10.1109/KhPIWeek61436.2025.11288666.

[6] M. Safril, S. Hasan, and M. D. J. Siburian, "Battery management system on competition electric car," in *2024 8th Int. Conf. Electr., Telecommun. Comput. Eng. (ELTICOM)*, Medan, Indonesia, 2024, pp. 176–182. doi: 10.1109/ELTICOM64085.2024.10864777.

[7] N. Banerjee, S. Ghosh, S. Borah, G. Aarthi, C. A, and A. G, "Solar light tracking with STM32 and IoT integration," in *2025 Int. Conf. Sens. Relat. Netw. (SENNET) Special Focus Digit. Healthc.*, Vellore, India, 2025, pp. 1–6. doi: 10.1109/SENNET64220.2025.11135966.

[8] M. G. Romero-Sánchez, O. Rodriguez-Abreo, J. M. Juarez-Lopez, A. A. Ortiz-Verdin, O. Martinez-Guzman, and J. D. C. Irineo, "Development of a solar panel monitoring system for power and visible light using Arduino and INA219/BH1750 sensors," in *2025 22nd Int. Conf. Electr. Eng., Comput. Sci. Autom. Control (CCE)*, Mexico City, Mexico, 2025, pp. 1–5. doi: 10.1109/CCE67728.2025.11272019.

[9] D.-J. Wang, Y.-Y. Fanjiang, J. T. K. Xiang, Y.-H. Wu, S.-A. Shen, and J.-Y. Tsai, "Performance evaluation of micro power systems with MQTT-based monitoring," in *2025 IEEE 14th Global Conf. Consum. Electron. (GCCE)*, Osaka, Japan, 2025, pp. 1144–1145. doi: 10.1109/GCCE65946.2025.11275017.

[10] R. M. Crowter and N. Saeed, "Design and implementation of a simple wireless battery monitoring system for photovoltaic applications," in *2023 IEEE 9th World Forum Internet Things (WF-IoT)*, Aveiro, Portugal, 2023, pp. 1–6. doi: 10.1109/WF-IoT58464.2023.10539503.

[11] Y. Sari et al., "Comparing the accuracy of INA219, PZEM-004T, and MAX471 sensors for measuring current and voltage of Internet of Things-based solar panels," in *2024 Ninth Int. Conf. Inform. Comput. (ICIC)*, Medan, Indonesia, 2024, pp. 1–6. doi: 10.1109/ICIC64337.2024.10956405.

[12] A. Maroşan, G. Constantin, C. E. Gîrjob, A. L. Chicea, and M. Crenganiş, "Real time data acquisition of low-cost current sensors ACS712-05 and INA219 using Raspberry Pi, DAQCplate and Node-RED," *Proc. Manuf. Syst.*, vol. 18, no. 2, pp. 51–59, 2023.

[13] V. Gaikar, R. Deshmukh, T. Kumar, S. Chowdhury, Y. Sesharao, and Y. Abilmazhinov, "IoT based solar energy monitoring system," *Mater. Today: Proc.*, vol. 80, pp. 369–374, 2021. doi: 10.1016/j.matpr.2021.07.364.

[14] M. F. Hakim, I. Ridzki, I. Su'Udi, A. Setiawan, W. Kusuma, and T. U. Syamsuri, "IoT-based monitoring and controlling system for energy consumption costs from battery supply," *J. Rekayasa Elektrika*, vol. 20, no. 4, pp. 202–209, Dec. 2024. doi: 10.17529/jre.v20i4.35237.

[15] K. Luechaphonthara and A. Vijayalakshmi, "IOT based application for monitoring electricity power consumption in home appliances," *Int. J. Electr. Comput. Eng. (IJECE)*, vol. 9, no. 6, pp. 4988–4992, Dec. 2019. doi: 10.11591/ijece.v9i6.pp4988-4992.

[16] A. Salunkhe, Y. Kanse, and S. Patil, "Internet of Things based smart energy meter with ESP 32 real time data monitoring," in *2022 Int. Conf. Electron. Renew. Syst. (ICEARS)*, Tuticorin, India, 2022, pp. 446–451. doi: 10.1109/ICEARS53579.2022.9752144.

[17] A. Patel, S. Sharma, Z. Siddique, and P. S. Mahajani, "A peer-to-peer decentralized smart energy grid," in *2025 12th Int. Conf. Emerg. Trends Eng. Technol. - Signal Inf. Process. (ICETET - SIP)*, Nagpur, India, 2025, pp. 1–6. doi: 10.1109/ICETETSIP64213.2025.11156685.

[18] Texas Instruments, "INA219 Zero-Drift, Bidirectional Current/Power Monitor With I2C Interface," SBOS448G datasheet, Dec. 2015. [Online]. Available: https://www.ti.com/lit/ds/symlink/ina219.pdf

[19] Espressif Systems, "ESP32-C6 datasheet," Version 1.4, 2023. [Online].

Available: https://documentation.espressif.com/esp32-c6_datasheet_en.html

[20] Texas Instruments, "INA219 Zero-Drift, Bidirectional Current/Power Monitor With I2C Interface," Rev. C, Dallas, TX, 2015. [Online]. Available: https://www.ti.com/lit/ds/symlink/ina219.pdf

[21] B. Han, S. Wu, J. Li, K. Wang, and X. Cai, "A novel driving ultrasonic atomizer based on class-E amplification circuits," in *2024 IEEE 2nd Int. Conf. Control, Electron. Comput. Technol. (ICCECT)*, Jilin, China, 2024, pp. 404–407. doi: 10.1109/ICCECT60629.2024.10546119.

[22] J. Ding, *MATLAB Scientific Plotting and Data Analysis*. Amsterdam, The Netherlands: Elsevier, 2025. doi: 10.1016/C2024-0-03625-9.

[23] F. Nelli, *Python Data Analytics: With Pandas, NumPy, and Matplotlib*, 3rd ed. New York, NY, USA: Apress, 2023. doi: 10.1007/978-1-4842-9532-8.

[24] M. D. F. McInnes and P. M. M. Bossuyt, "Understanding test accuracy measures," in *Cochrane Handbook for Systematic Reviews of Diagnostic Test Accuracy*, J. J. Deeks, P. M. M. Bossuyt, M. M. Leeflang, and Y. Takwoingi, Eds. Hoboken, NJ, USA: Wiley, 2024, ch. 4. doi: 10.1002/9781119756194.ch4.

[25] P. Royston, "An extension of Shapiro and Wilk's W test for normality to large samples," *Appl. Statist.*, vol. 31, no. 2, pp. 115–124, 1982. doi: 10.2307/2347973.

[26] R. Chattamvelli and R. Shanmugam, *Descriptive Statistics for Scientists and Engineers: Applications in R*, 2nd ed. Cham, Switzerland: Springer, 2023, ch. 4. doi: 10.1007/978-3-031-32330-0.

[27] A. J. Lari, A. P. Sanfilippo, D. Bachour, and D. Perez-Astudillo, "Using machine learning algorithms to forecast solar energy power output," *Electronics*, vol. 14, no. 5, p. 866, Feb. 2025. doi: 10.3390/electronics14050866.

[28] P. Schober, C. Boer, and L. A. Schwarte, "Correlation coefficients: Appropriate use and interpretation," *Anesth. Analg.*, vol. 126, no. 5, pp. 1763–1768, May 2018. doi: 10.1213/ANE.0000000000002864.

[29] A. F. Siegel, "Variability: Dealing with diversity," in *Practical Business Statistics*, 7th ed., A. F. Siegel, Ed. Cambridge, MA, USA: Academic Press, 2016, ch. 5, pp. 101–128. doi: 10.1016/B978-0-12-804250-2.00005-5.

[30] U. Ejder and S. A. Özel, "A novel distance-based moving average model for improvement in the predictive accuracy of financial time series," *Borsa Istanbul Rev.*, vol. 24, no. 2, pp. 376–397, Mar. 2024. doi: 10.1016/j.bir.2024.01.011.